Fuel Processing Technology 118 (2014) 310–317

Contents lists available at ScienceDirect

Fuel Processing Technology

journal homepage: www.elsevier.com/locate/fuproc

Combustion characteristics of biodiesel fuel in high recirculation conditions

V. Mahendra Reddy [a], Pratim Biswas [b], Prateek Garg [a], Sudarshan Kumar [a,*]

[a] Department of Aerospace Engineering, Indian Institute of Technology Bombay, Powai, Mumbai 400 076, India
[b] Department of Energy, Environmental & Chemical Engineering, Washington University at St. Louis, USA

ARTICLE INFO

Article history:
Received 2 January 2013
Received in revised form 14 July 2013
Accepted 10 October 2013
Available online 6 November 2013

Keywords:
Biodiesel combustion
Preheated air combustion
Liquid fuel combustion
Swirl combustion
Low emission burner

ABSTRACT

The potential of biodiesel as an alternative fuel for various applications leads to an investigation to understand the combustion characteristics of pure and blended biodiesel. The concept of internal recirculation of combustion products is employed in a high swirl and low emission burner to reduce emissions. Due to high boiling point (613 K) and SMD (37 μm) of biodiesel, air preheating with minimum temperature above the boiling point of biodiesel is considered. Air at different temperatures of 623, 673 and 703 K is injected tangentially. Swirl flow pattern in the combustor creates the central low pressure zone due to vortex breakdown and improves the recirculation of combustion products. Results in improved mixing and high residence time of reactants. Biodiesel is blended with diesel to reduce the surface tension and viscosity and improve the combustion characteristics. Literature has little consensus on NOx emissions from the combustion system operating with biodiesel. Therefore, the present study aims to reduce the thermal NO formation through the concept of exhaust gas recirculation. The CO, HC, NOx emissions and soot-volume fraction from biodiesel (100B0D), 50% blending (50B50D), diesel and kerosene are compared at different air preheating temperatures. A drastic reduction in emissions is observed in 50B50D as compared with pure biodiesel.

1. Introduction

The increased demand for energy is putting additional pressure on fossil fuel resources leading to early depletion of these resources [1–3]. Therefore, there is a great need to develop alternate resources and methods to fill the increasing energy demand of human civilization. Various bio-fuel energy resources such as biomass, biogas, vegetable oils, biodiesel, etc. are being explored as alternate sources of energy. These alternate energy resources are considered as environment-friendly [4,5]. Biodiesel has immense potential for being used as an alternate fuel to the conventional or fossil diesel for industrial heating applications, transportation, power generation and internal combustion engines. These biofuels are renewable, biodegradable, oxygenated and expected to help in reducing green-house gas (GHG) emissions [6–14]. There is little consensus on the effects of biodiesel on NOx emissions. However, as extensive literature indicates, a slight increase in emissions of nitrogen oxides (NOx) has been observed [9–14]. Blending of biodiesel reduces the NOx formation [10,15]. Biodiesel and its blends with diesel can be used in diesel engines without modifications because of similarities with diesel properties [1,6,8,10]. Espadafor et al. [10] have conducted experimental investigation to reduce the emissions of NOx on a 4-strock single-cylinder engine with the method of EGR (exhaust gas recirculation), however internal recirculation has little viability in IC engines due to various constraints. Extensive literature is available for high pressure conditions in IC engines [3–14]. However, very little work has been reported in the field of continuous combustion systems, such as gas turbine combustors and industrial heating applications. Recently, Chong and Hochgreb [16], and Bolszo and McDonnell [17] have experimentally studied the combustion characteristics of biodiesel in an open can-type gas turbine combustor configuration. Chong and Hochgreb [16] have investigated the combustion characteristics of palm biodiesel in swirl flow type cylindrical quartz combustor. A plain-jet air-blast atomizer is used for fuel injection. The main air flow is heated by two in-line air heaters (750 W) arranged in a series to simulate the high temperature conditions similar to that of a gas turbine combustor. The burner plenum and body are additionally heated by three Omega rope heaters (500 W) and insulated with high temperature heat-resisting materials to reduce heat loss. The heating facility allows the main air to be preheated to a temperature of 623 K. More investigations are required to study the evaporation and combustion characteristics of these biodiesel based fuels in order to understand the emissions characteristics from the combustion of these fuels. Therefore, in the present work, detailed combustion studies have been carried out in a high swirl combustor with air preheating to assess the emissions from the combustion of such fuels at conditions similar to those existing in gas turbine and industrial heating applications [17]. Internal recirculation of combustion products due to high swirl results in the dilution and preheating of fresh reactants that helps in suppressing the formation

* Corresponding author. Tel.: +91 22 2576 7124; fax: +91 22 2572 2602.
E-mail address: sudar@aero.iitb.ac.in (S. Kumar).

0378-3820/$ – see front matter © 2013 Elsevier B.V. All rights reserved.
http://dx.doi.org/10.1016/j.fuproc.2013.10.004

of thermal NO and CO emissions [18–26]. This motivated the authors to study the combustion and emission characteristics of biodiesel with the concept of recirculation of hot combustion products for reducing the emissions.

The process of combustion of liquid fuels is very complex due to the involvement of many processes such as atomization, droplet evaporation, mixture formation and subsequent combustion reaction. A brief summary of various liquid fuels having different properties is given in Table 1. The Sauter mean diameter (SMD) of the droplets in the spray is a function of surface tension (σ) and viscosity (μ) of the fuel [17,27]. At an injection pressure of $\Delta P = 9$ bar, the SMD of biodiesel spray is 37 μm. At the same injection pressure, the SMD of kerosene and diesel sprays are 20 and 26 μm respectively. Evaporation rate of droplets is a function of surface area to volume ratio (A_s/V) of droplet [28]. The A_s/V ratio of the biodiesel droplets is 1.62×10^5, whereas for kerosene droplets it is 3×10^5. The time required for droplet evaporation increases with an increase in the droplet diameter (SMD) [29]. With an increase in the evaporation time, species mixing and flame stabilization become more difficult. Evaporation rate of biodiesel droplets is relatively very small because of high boiling point of biodiesel. In the case of conventional combustion, flame stabilizes in a narrow zone near the fuel nozzle resulting in the formation of a high temperature zone near the nozzle exit. Due to this, fuel droplets evaporate quickly in the conventional combustion mode and get combusted near the nozzle exit [30]. However, in the case of recirculation of hot combustion products, reaction zone is distributed throughout the volume of the chamber [18,22]. The peak flame temperature and its fluctuations are relatively lower compared to those in the conventional combustion mode [18–22,25]. The droplet evaporation rate is expected to be higher in this mode compared to that in the conventional combustion mode due to the higher average temperature in the combustor [30].

In the present study, detailed combustion and emission characteristics of biodiesel and its blends have been studied in a swirl flow combustor configuration with the concept of internal recirculation of combustion products. A two stage combustor configuration with 19 kW thermal input and heat release density of ~4.8 MW/m^3 is used as shown in Fig. 1a. Tangential air injection scheme is used to achieve swirl flow pattern in the combustor. The concept of swirl stabilized flame is commonly used [31–34] to achieve high mixing levels and high residence time. The details of design methodology of the present combustor have been discussed in Reddy et al. [33]. Initial experiments showed that it was not possible to achieve low emission combustion mode with biodiesel for ambient conditions (300 K) due to the high boiling point of biodiesel. This necessitated air-preheat to a temperature close to the boiling point of biodiesel (~613 K). Therefore, the initial air-preheat temperature is maintained at 623 K. The capacity of the present air preheater is sufficient to preheat the air supply up to 710 K at all equivalence ratios ($\Phi = 1$ to 0.45). Therefore three preheat temperature conditions of 623, 673 and 703 K are considered in this study. Air preheating improves the evaporation rate of biodiesel droplets as the rate of evaporation of biodiesel is less than half that of kerosene fuel. An electrical air preheater with a variable heating capacity of 3 to 8 kW is installed on the primary line before the combustor inlet; the location of the air preheater is shown in Fig. 1b. Biodiesel is blended with diesel for certain studies to understand the effect of blending on the combustion process and emissions [35–37]. Three different fuel combinations are tested in this study, 100% biodiesel, 50% blending with diesel (50B50D), and pure diesel. Temperature distribution in the combustor, exhaust gas temperature and emissions are compared for different operating conditions and different fuels.

Table 1
Characteristic details of different fuels.

Property	Kerosene	Diesel	Biodiesel
Density (kg/m^3)	800	860	890
Kinematic viscosity, ν (m^2/s)	2.71×10^{-6}	3.64×10^{-6}	5.27×10^{-6}
Surface tension, σ (mN/m)	25	23	30.55
Flash point (K)	334	398	429
Boiling point (K)	433	558	613
SMD (μm) ($\Delta P = 9$ bar)	20	26	37
Ratio of surface area to volume (m^{-1}) (A_s/V)	300,000	230,769	162,162
Evaporation time (ms) (τ_{evap})at $T_\infty = 1000$ K	8.1	11.6	18.9

2. Experimental setup

Fig. 1 shows a schematic diagram of the experimental setup and dimensional details of a typical two-stage combustor. The combustor is placed vertically on a test stand as shown in the figure. Biodiesel is stored in a pressurized steel tank. A ball valve is inserted in the line between fuel tank and fuel nozzle. The fuel flow is controlled through a ball valve during the combustor operation. A pressure swirl injector with a mass flow rate of 1.78 kg/h at $\Delta P = 9$ bar is mounted centrally at the bottom of the combustor. The spray cone angle of the injector is 45°, and the SMD at $\Delta P = 9$ bar is in the range of 36–39 μm (measured with Malvern Mastersizer). The spray characteristics are measured at a retraction position of 120 mm from the orifice of the nozzle. The air is drawn from a high pressure storage tank and controlled through electric mass-flow controllers (500 and 1000 SLPM). Preheating in the secondary chamber is not considered because partially combusted species and evaporated fuel from the primary chamber achieve a sufficiently high temperature to ensure the continuation of the combustion reaction in the secondary chamber. Clockwise air injection and counterclockwise fuel swirl scheme is used for quick evaporation and increased mixing of fuel droplets with the incoming fresh air [27]. For all operating conditions, the air inlet diameter (5 mm) of tangential ports is maintained constant. An electrical air preheater with a variable heating capacity of 3 to 8 kW is installed on the primary air line near the combustor inlet. The location of the air preheater is shown in Fig. 1b. Air preheating temperature is controlled through an auto temperature controller circuit. Preheated air is supplied to the primary chamber and air at ambient conditions is supplied to the secondary chamber. For stoichiometric combustion, 95% of the air is injected in the primary chamber and the remaining 5% is injected in the secondary chamber. For lean combustion cases, 50% of the excess air along with the stoichiometric air is injected into the primary chamber. The remaining 50% of excess air is injected into the secondary chamber. The combustor is initially ignited with spark-plug and run with premixed liquefied petroleum gas (LPG)–air mixture. To ensure initial flame stabilization, the stoichiometric flow rates of biodiesel and air are maintained. The exhaust gas composition is measured with QuintoxKM-9106 gas analyzer and normalized to 15% O_2 level in the exhaust. The accuracy of the sensors in the gas analyzer with an O_2 analyzer(0–25% range, 0.1% accuracy), CO analyzer (0–10,000 ppm range, accuracy ±5% of reading),NO analyzer (0–5000 ppm, ±5 ppm accuracy), a HC (hydrocarbon) analyzer (0–50,000 ppm), and a CO_2 analyzer. Continuous online measurement of the sample gas has been carried out. Temperature measurements are carried out with Omega KMTXL-040 (diameter = 1 mm) type thermocouple, with a maximum measured temperature range of 1600 K. The measured temperature is corrected for conduction and radiation losses from the thermocouple junction [38]. A photograph of the soot volume fraction measurement system is shown in Fig. 1c. The soot volume fraction has been measured using the technique of carbon balance method of Choi et al. [39], the accuracy of the instrument is ±1%. The sampling tube is placed at the outlet of the combustor and is connected to the filter paper assembly through flexible piping which is subsequently connected to vacuum pump with rotameter (0–30 SLPM). The flow rate of 12–14 LPM is maintained during the experiment based on limiting flow rates provided by the manufacturer of the micro glass fiber filter paper (99% collection efficiency and 0.1 μm retention size). The time of soot collection is also

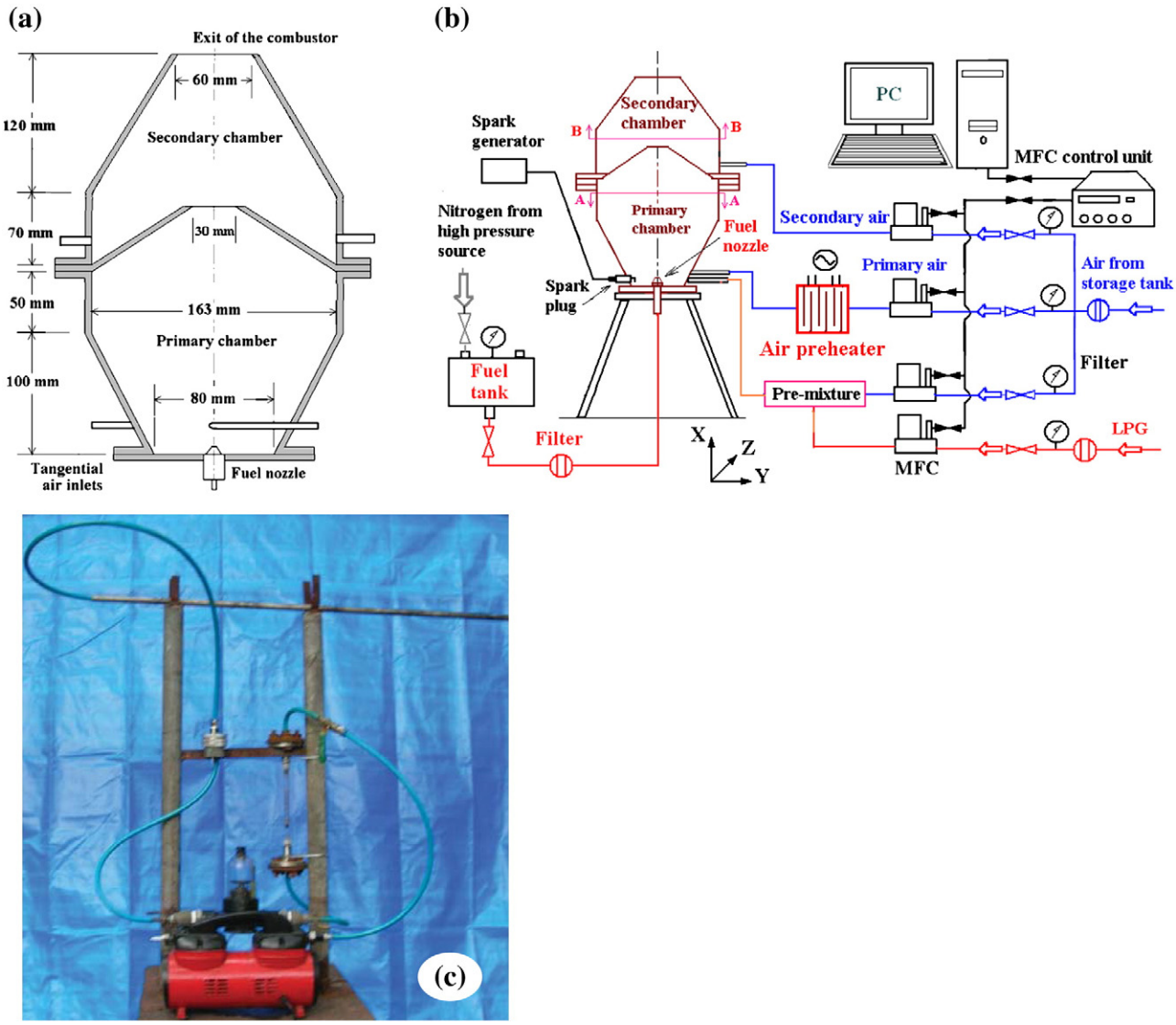

Fig. 1. (a) Schematic diagram of two stage combustor. (b) Experimental setup details. (c) Setup for the soot-volume fraction measurement.

monitored. After collection of soot sample for 180 s, the filter paper is removed from the assembly and it is weighed on a micro balance.

3. Reactant dilution ratio (R_{dil})

Internal recirculation of combustion products is an effective method to suppress the CO and thermal NO formation [18,20,22]. Therefore, reacting flow computational studies are carried out to maximize the recirculation of hot combustion products and understand the flow features inside the combustors with high swirl conditions. Previous studies of Reddy et al. [33] have considered a two stage combustor configuration with three different combustor configurations of D60, D45 and D30. Computational analysis shows that D30 is an optimal configuration for achieving flameless combustion with ultra-low emissions. The same combustor (D30) is considered in this study with biodiesel as liquid fuel. A general purpose CFD code Fluent 6.3 is used for the computational studies in the present work. The computational mesh is generated in Gambit 2.3. Three-dimensional Navier–Stokes equations are discretized in the physical domain and then solved using finite-volume based method. The Reynolds stress model (RSM) is used for turbulence modeling. The energy equation is solved considering 20 intermediate species equilibrium chemistry and non-premixed droplet combustion model for simulating the combustion of the liquid fuels. A 3-D double precision pressure-based solver is used. Compressible flow is considered and the viscosity is calculated using Sutherland's law. Specific heats were defined as a function of the temperature (piecewise polynomial). P1 radiation model is used. Sunflower oil, a variant of the biodiesel ($CH_{1.67}O_{0.22}N_{0.058}$) [39] is considered as fuel with a density of 890 kg/m^3. The density of the present biodiesel is the same as fuel used in the experiments of Gercel [40] and Ilkılıç et al. [41]. Oxygen in the fuel (biodiesel) is considered. The amount of O_2 in the fuel is added to the oxidizer quantity while calculating the equivalence ratio. Based on this calculation, air mass flow rate through the inlet is fixed. Fuel injection is simulated as a solid cone type spray with a spray cone angle of 45°. A uniform diameter droplet combustion model is assumed. Air is injected through four tangential inlets at the bottom of the chamber. A constant mass flow inlet condition normal to the boundary surface is applied at the tangential air inlets. A pressure outlet based boundary condition is applied at the exhaust port. No slip wall and constant temperature boundary conditions are applied at the walls. The solution is considered to be converged when RMS residuals of the flow, species and energy balance of the system are of the order of 10^{-5} and 10^{-6}, respectively. A number of computations were carried out using tetra mesh with different mesh sizes of 2.5, 2.0, 1.5, and 1.2 mm respectively. The number of cells for computations was varied from 1.5 to 4.0 million

elements. Grid converged for a mesh size of 1.5 mm with approximately 3.0 million grid points. The grid convergence is calculated based on the Grid Convergence Index (*GCI*) criteria (Reddy [42] and Manna et al. [43]). If the *GCI* for two successive grid sizes is below 3%, it can be considered that grid convergence has been achieved (Manna et al. [43]).

The variation of reactant dilution ratio for different equivalence ratios is analyzed and shown in Fig. 2a (D30 combustor). The reactant dilution ratio (R_{dil}) is the ratio of net mass flow rate interaction in a plane to the total mass flow rate of the reactants. It is a measure of the recirculation of the combustion products and their interaction with the fresh mixture [33]. The reactant dilution ratio is calculated as follows.

$$R_{dil} = \frac{\dot{m}_{axial} - \left(\dot{m}_{ox} + \dot{m}_f\right)}{\left(\dot{m}_{ox} + \dot{m}_f\right)}$$

$$\dot{m}_{axial} = \iint \rho v_{axial}\, dydz$$

Here $\dot{m}_{axial}$ is total mass flow interacting at a given plane, $\dot{m}_{ox}$ and $\dot{m}_f$ are the mass flow rates of oxidizer and fuel respectively. ρ and v_{axial} are the density and axial velocity.

The reactant dilution ratio, R_{dil} and zone length of high recirculation increases with a decrease in the global equivalence ratio. The maximum dilution ratio plane shifts towards the upstream direction with a decrease in the equivalence ratio. With a decrease in the global equivalence ratio, air mass flow rate and inlet air velocity are increased. High velocity in the near wall region and high negative velocity at central zone of the combustor is observed for lower equivalence ratios as shown in Fig. 2. The recirculation rate increases due to the large negative velocity at the central zone. At a radial position of 0.035 m (at an axial position of 0.07 m), the negative velocities are −6, −17, −21, −24 and −27 m/s for equivalence ratios of 0.98, 0.73, 0.61, 0.52, and 0.46 respectively, indicating the increase in the recirculation of hot combustion products with a decrease in the global equivalence ratio as shown in Fig. 2b.

4. Results and discussion

4.1. Temperature distribution

Temperature distribution at different radial locations in the primary and secondary chambers is measured for different fuels and various air preheating temperatures, as shown in Fig. 3. Locations of temperature measurement, A–A and B–B are shown in Fig. 1b. Temperature distribution measurements are carried out for an air preheat temperature of 703 K and global equivalence ratio of 0.92. Because of the lower evaporation rate of biodiesel and blended biodiesel (50B50D) droplets, a large temperature gradient is observed in the primary chamber. The temperature difference between the near wall region to the center of the combustor (ΔT) for kerosene and diesel fuels are 356 and 405 K respectively. The temperature difference for blended biodiesel (50B50D) and pure biodiesel increases to 689 and 827 K respectively, indicating that the combustion process increasingly becomes localized near the center for biodiesel fuel. The total energy release for biodiesel and blended biodiesel in the primary chamber is relatively small compared to kerosene and diesel fuels. By contrast, the total energy release for biodiesel and blended biodiesel in the secondary chamber is higher. This is due to the reason that large droplets from the spray of the biodiesel partially evaporate in the primary chamber resulting in partial combustion and large temperature difference. Complete combustion is achieved in the secondary chamber with the remaining part of the evaporated fuel vapor and secondary oxidizer. The temperature gradient in the secondary chamber for biodiesel is relatively small and comparable to kerosene and diesel fuels. It is observed that for kerosene and diesel combustion, almost complete combustion occurs in the primary chamber and a very small fraction of unburned fuel burns in the secondary chamber [33]. The near wall and axis temperature difference in the secondary chamber for kerosene, diesel, biodiesel and blended biodiesel (50B50D) are relatively small, for instance, 351, 383, 257, and 319 K, respectively as shown in Fig. 3b. It is to be noted here that the secondary air enters the secondary chamber at ambient conditions.

4.2. Emission analysis

4.2.1. CO and HC emissions

Emissions of CO and HC are measured with Quintox KM-9106 gas analyzer for different operating conditions as shown in Fig. 4. Although it has been reported in the literature that CO emissions increase for lean operation [44,45], in the present work, in the case of biodiesel, CO emissions are reduced as global equivalence ratio is reduced from $\Phi = 1.0$ to 0.6 and then increased till $\Phi = 0.45$. This is due to the requirement of increased heat input for preheating the incoming fresh air with a decrease in the global equivalence ratio. The total heat release, Q_T (sum of chemical heat input, Q_C and heat input through air preheating, Q_T) from the combustor increases with a decrease in the mixture equivalence ratio. However, the heat release per unit mass of fuel-air mixture ($\dot{Q}_{mix}$) decreases and leads to a lower flame temperature as shown in Fig. 5. The CO oxidation process occurs rapidly in the presence of hydroxyl radical (OH) [46]. A large OH radical pool is

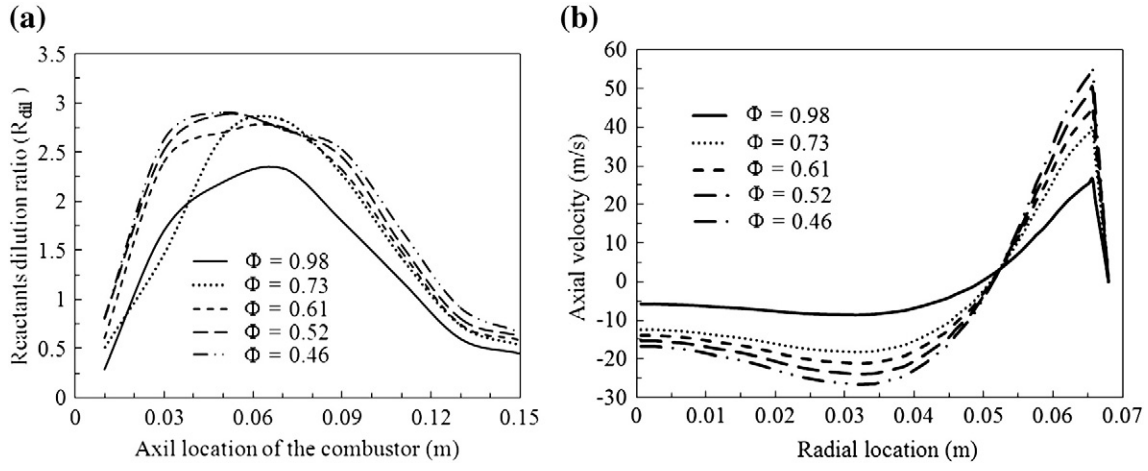

Fig. 2. (a) Variation of reactant dilution ratio for different equivalence ratios, (b) axial velocity distribution at an axial position of 0.07 m for different equivalence ratios.

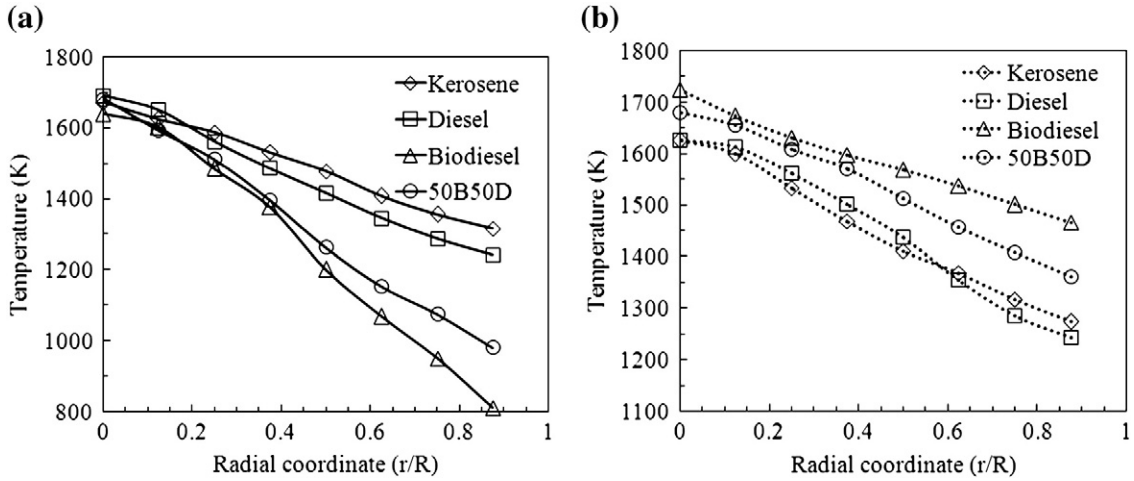

Fig. 3. Radial temperature distribution for different fuels in (a) primary and (b) secondary chambers at A–A and B–B planes.

sustained in the high temperature combustion zone and the time required for CO oxidation decreases with an increase in the local temperature [45]. High temperature in the combustor enhances the droplet evaporation and oxidation of CO resulting in reduced CO emissions. For very lean mixtures (Φ varying from 0.6 to 0.45), the flame temperature is relatively very small resulting in a reduction in the CO oxidation rates. For instance, the adiabatic flame temperature (calculated using CEA equilibrium program) of air–fuel mixture for a preheat temperature of 703 K and equivalence ratios of 0.6 and 0.45 are 2039 and 1760 K respectively. This reduces the droplet evaporation significantly, resulting in slow oxidation of CO (lack of OH) in the combustion zone. For the combustor operation in very lean equivalence ratios, the reactant dilution ratio is increased, as shown in Fig. 2a. Large preheating is required for sustaining a stable and complete combustion with high reactant dilution ratios (large recirculation) [18]. With a decrease in the global equivalence ratio, the oxidizer is diluted more and the mixture (fresh oxidizer and recirculated combustion products) is not heated to the required level due to lower heat release in the combustor. This results in incomplete combustion leading to an increase in the CO emissions for very low equivalence ratios. It has been observed during the experimental investigations that flame blowoff occurs with global equivalence ratio, Φ below 0.45. For biodiesel fuel with an air preheat temperature of 703 K, the CO emissions are observed to be 1834 ppm at Φ = 0.98 and these emissions continuously reduce to 1312 ppm with a decrease in global equivalence ratio till Φ = 0.56. The CO emissions again increase to 1813 ppm with a further decrease in the equivalence ratio (Φ = 0.56 to 0.45). At Φ = 0.61, the CO emissions for different preheat temperatures of 623, 673 and 703 K are 1654, 1547 and 1401 ppm, respectively. This indicates that the CO emissions decrease with an increase in the air preheat temperature.

The viscosity, surface tension and boiling temperature of biodiesel can be reduced by blending it with conventional diesel fuel. Due to this, the droplet size (SMD) is reduced and the evaporation rate increases [35,37] resulting in better performance of the combustor and lower emissions are expected from such blended fuels. The CO emissions for blended fuel (50B50D) are reduced drastically compared to those of pure biodiesel. At Φ = 0.61, the CO emissions for 50B50D fuel are 351, 116 and 69 ppm, respectively at preheat temperatures of 623, 673 and 703 K, respectively. The trend of variation of CO emissions with global equivalence ratio is similar to that of pure biodiesel as seen in Fig. 4a. The emissions of unburned hydrocarbons are measured for all the operating conditions. HC emissions decrease with a decrease in the global equivalence ratio and increase in the air preheat temperature as shown in Fig. 4b. In the case of pure biodiesel with an air preheat temperature of 703 K, 171 ppm of HC is observed at Φ = 0.61. Under the same conditions, a lower level of HC emissions, 65 ppm, is observed for blended biodiesel (50B50D).

4.2.2. NOx emissions

The variation of NOx emissions with fuel blending and air preheating is shown in Fig. 6. Increased internal recirculation of hot combustion

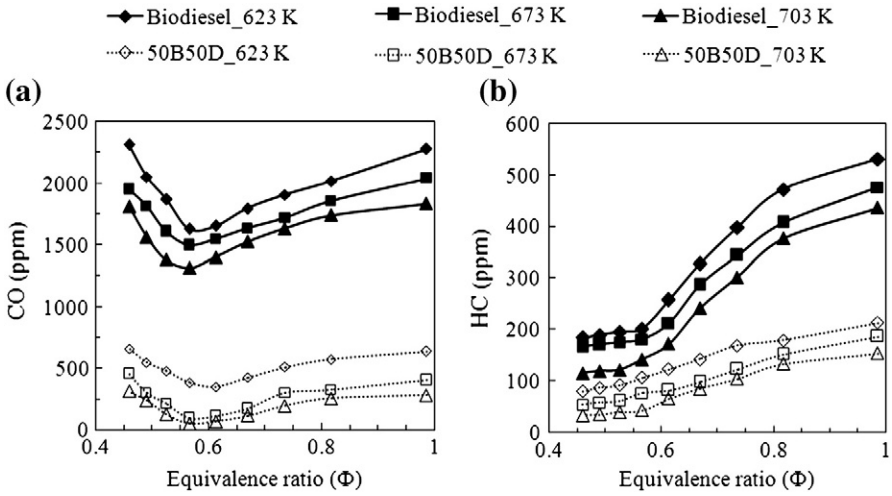

Fig. 4. Variation of emissions with equivalence ratio for different preheat and fuel conditions (a) CO and (b) HC.

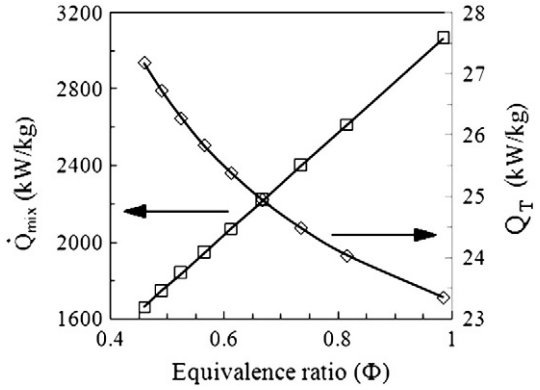

Fig. 5. Variation of total heat release from the combustor and heat release per unit mass of air fuel mixture with equivalence ratio.

products in the present combustor configuration distributes the reaction zone within the combustor volume resulting in a lower peak temperature [18,22,47]. This suppresses the formation of NOx through the thermal route. Hence, very low NOx emissions are observed in the present experiments. External preheating of the air as well as internal preheating and dilution of the oxidizer due to the recirculation of hot combustion products leads to improved droplet evaporation rate, enhanced mixing of species and distributed reaction zone. This results in a more uniform temperature profile with reduced temperature fluctuations in the combustor and reduced NOx formation through the thermal route [18]. At a global equivalence ratio of $\Phi = 0.61$ and air preheat temperatures of 623, 673 and 703 K, NOx emissions are 72, 64, and 55 ppm, respectively. For lean equivalence ratios, the peak temperature in the combustion zone is relatively lower resulting in a decrease in the NOx emissions. For $T_{air} = 703$ K, NOx emissions are reduced from 91 to 35 ppm with a reduction in equivalence ratio, Φ from 0.98 to 0.45. In the case of 50B50D blended biodiesel, lower NOx emissions were observed compared to pure biodiesel. This is because of reduced SMD and increased evaporation rate along with rapid mixing and distribution of reaction leading to a more uniform temperature distribution in the combustion chamber as discussed in Fig. 3. For an equivalence ratio of $\Phi = 0.61$ and air preheat temperature of 623, 673 and 703 K, the NOx emissions are 22, 19, and 16 ppm, respectively. The emissions from the combustion of pure diesel and kerosene fuel in the same combustor have been measured for an air preheat temperature of $T_{air} = 703$ K, and plotted in Fig. 6 for comparison purposes. Very low NOx emissions are observed for all equivalence ratios as compared to pure biodiesel and blended biodiesel (50B50D) at all air preheat temperature conditions. The comparison of NO emissions for pure and blended biodiesel fuels shows that it achieves a combustion mode similar to that of flameless combustion mode in terms of emission performance (Fig. 7). However, visual observations showed that most of the combustion zone remained pale yellow for pure biodiesel combustion. For blended 50B50D biodiesel, partial flameless combustion was achieved which showed a very small zone of pale yellow wick type flame stabilized at the center of the combustor. The extent of yellowish flame reduced with an increase in diesel blending. Complete flameless combustion mode is achieved on the same combustor with kerosene, diesel and gasoline fuels [34].

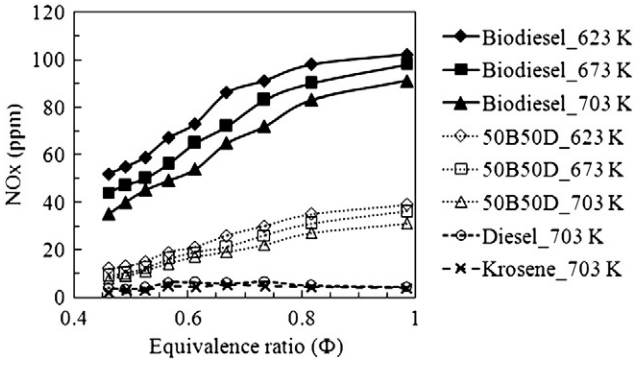

Fig. 6. Variation of NOx emissions with fuel blending and air preheating.

4.3. Comparison of emissions

The emissions from the combustion of various fuels are compared with the existing literature and shown in Fig. 7. In the present study, combustion characteristics of kerosene and diesel have also been included for comparison purposes with an air preheat temperature of $T_{air} = 703$ K. The CO and NOx emissions for four fuels; pure biodiesel, blended biodiesel (50B50D), kerosene and diesel with air preheat temperature of 703 K are compared with the emissions of kerosene fuel ($T_{air} = 300$ K) in flameless combustion mode (Reddy et al. [33]) and Swirl combustor configuration of Chong and Hochgreb [16]. The detailed comparison is shown in Fig. 7a and b. It is to be noted that emissions are plotted on a logarithmic scale. The CO emissions of Chong and Hochgreb [16] at $\Phi = 0.4$ for palm biodiesel are 57 ppm. These emissions of CO compare well with those of the blended biodiesel (50B50D) (51 ppm at $\Phi = 0.56$). For kerosene and diesel, very low CO emissions of 6 and 9 ppm respectively are measured at $\Phi = 0.61$. These emissions are relatively very small as compared to flameless combustion with kerosene fuel (Reddy et al. [33]). From this comparison, it is clear that air preheating improves the evaporation characteristics of kerosene and diesel fuel droplets resulting in improved combustion and further reduction in the emissions from the combustor. NOx emissions from the swirl combustor of Chong and Hochgreb [16] at $\Phi = 0.4$ are 220 ppm. However, in this present combustor, for biodiesel, comparatively much lower NOx emissions (97 ppm at $\Phi = 0.61$) are observed. For 50B50D, diesel and kerosene fuels, the NOx emissions are 21, 5, and 4 ppm, respectively ($\Phi = 0.61$). The recirculation of the hot combustion products results in significant reduction of CO and NOx emissions compared to the conventional combustion modes [16]. Oxidizer preheating improves the flame stability under lean conditions and emissions are reduced due to a shift in the operation of the combustor from the conventional mode [16] to a mode with high recirculation of hot combustion products [33].

4.4. Soot volume fraction

The emissions of soot volume fraction from the exhaust of the combustor are measured using the carbon balance method of Choi et al. [39]. The variation of soot emissions with global equivalence ratio for different fuels and preheating conditions is shown in Fig. 8. Soot emissions are not normalized to 15% O_2 level. The figure reveals that, the equivalence ratio directly influences the formation of soot in the combustion system. As the global equivalence ratio is reduced, the soot volume fraction also decreases for various fuels (see Fig. 8). The formation of the soot is proportional to the average combustor temperature and it decreases with a decrease in the global equivalence ratio [48]. For pure biodiesel, higher soot emissions are observed compared to blended biodiesel (50B50D). It is perhaps due to the formation of large droplets leading to reduced evaporation and combustion rate of pure biodiesel fuel compared to 50B50D. It is interesting to note that air preheating considerably affects the formation of various pollutant emissions i.e. CO, HC and NOx. However, its influence on soot formation is very weak as seen in Fig. 8. Due to the smaller droplet size and high evaporation rate of kerosene and diesel fuels with uniform temperature distribution, very low levels of soot have been observed. The effect of global equivalence ratio on the soot emissions is very weak for kerosene and diesel fuels. At $\Phi = 0.61$ and

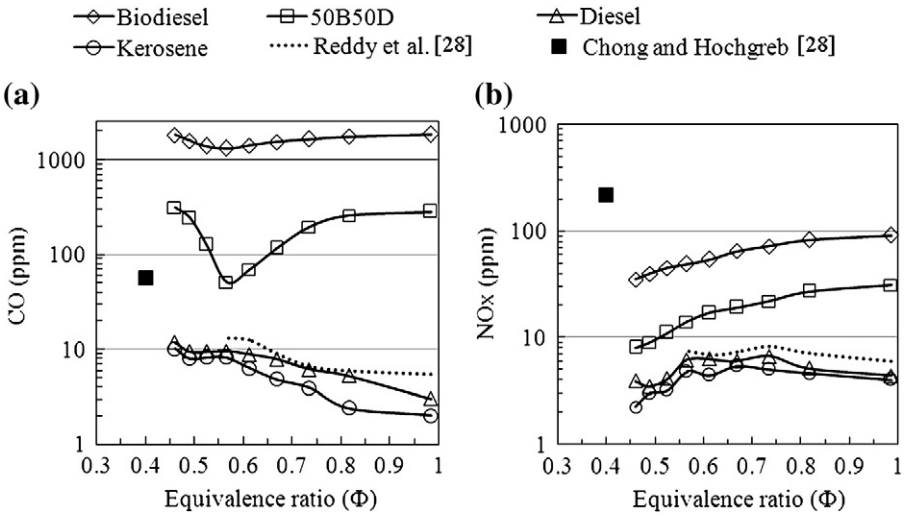

Fig. 7. Comparison of emissions for different fuels at an air preheat temperature of 703 K: (a) CO and (b) NOx.

703 K air preheat temperatures, the measured soot volume fractions are 3.1, 1.7, 0.7, and 0.6 ppm for biodiesel, 50B50D, diesel and kerosene, respectively.

5. Conclusions

In the present work, an effort has been made to understand the combustion of biodiesel fuel and its blends in a combustor configuration with preheated air and high swirl conditions. The combustion of biodiesel presents severe operational challenges due to its higher viscosity and higher boiling point resulting in lower evaporation and combustion rates. Some of these properties can be significantly improved by blending these biofuels with conventional fuels. Detailed measurements of emissions and combustion characteristics have been carried out for different fuels and air preheat conditions. The CO, HC and NO_x emissions for pure biodiesel are orders of magnitude higher compared to those of blended biodiesel, pure diesel and kerosene at different air preheat temperatures. At a particular operating condition, $\Phi = 0.61$, the CO emissions for pure biodiesel are 1401 ppm compared to 69 ppm for 50B50D with an air preheat temperature of 703 K. CO emissions of pure biodiesel are reduced significantly from 1654 ppm to 1401 ppm when the air preheating temperature is increased from 623 K to 703 K. Blending of these fuels also helps in reducing the emissions of NOx and unburned hydrocarbons. A comparison of combustor emissions with the literature shows that the emissions from the present combustion system are relatively much lower. Soot formation for pure biodiesel at all equivalence ratios is observed to be higher than for blended biodiesel (50B50D), kerosene, and diesel fuels. The air preheat temperature shows a weak effect on soot formation. Therefore, it is clear from the present study that blending of biodiesel with other combustible liquid fuels helps in significantly reducing the emissions without compromising the combustion completeness and emissions from the combustion systems. Partial blending of these biofuels with various fossil fuels such as kerosene and diesel will reduce the pollutant emissions significantly and enhance the combustion efficiency.

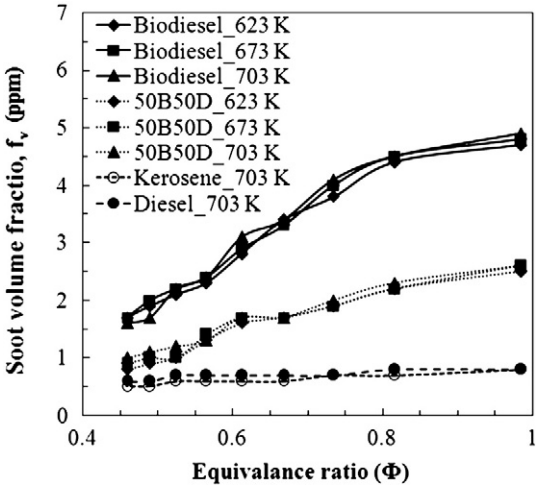

Fig. 8. Experimental measurement setup for soot volume fraction. Soot volume fraction for different fuel and preheating temperature conditions.

Acknowledgments

The authors would like to acknowledge the funding received for this work from MAGEEP (McDonnell Academy Global Energy and Environment Partnership) through the ACESS program.

References

[1] A.K. Agarwal, Progress in Energy and Combustion Science 33 (2007) 233–271.
[2] S.A. Basha, K.R. Gopal, S. Jebaraj, Renewable and Sustainable Energy Reviews 13 (2009) 1628–1634.
[3] M.N. Nabi, M.S. Akhter, M.M.Z. Shahadat, Bioresource Technology 97 (2006) 372–378.
[4] M.A. Gumus, Fuel 89 (2010) 2802–2814.
[5] X. Jinlin, T.E. Grift, A.C. Hansen, Renewable and Sustainable Energy Reviews 15 (2011) 1098–1116.
[6] C. He, Y. Ge, J. Tan, K. You, X. Han, J. Wang, Q. You, A.N. Shah, Atmospheric Environment 43 (2009) 3657–3661.
[7] M. Gumus, S. Kasifoglu, Biomass and Bioenergy 34 (2010) 134–139.
[8] S.H. Yoon, C.S. Lee, Fuel Processing Technology 92 (2011) 992–1000.
[9] E. Buyukkaya, Fuel 89 (2010) 3099–3105.
[10] F.J.J. Espadafor, M. Torres, J.A. Velez, E. Carvajal, J.A. Becerra, Fuel Processing Technology 103 (2012) 57–63.
[11] J.P. Szybist, J. Song, M. Alam, A.L. Boehman, Fuel Processing Technology 88 (2007) 679–691.
[12] M. Lapuerta, O. Armas, J.R. Fernandez, Progress in Energy and Combustion Science 34 (2008) 198–223.
[13] A.B. Koc, M. Abdullah, Fuel Processing Technology 109 (2013) 70–77.
[14] M.S. Graboski, R.L. McCormick, Progress in Energy and Combustion Science 24 (1998) 125–164.
[15] S.K. Hoekman, C. Robbins, Fuel Processing Technology 96 (2012) 237–249.
[16] C.T. Chong, S. Hochgreb, Combustion Science and Technology 184 (2012) 1093–1107.
[17] C.D. Bolszo, V.G. McDonnell, Proceedings of the Combustion Institute 32 (2009) 2949–2956.
[18] J.A. Wunning, J.G. Wunning, Progress in Energy and Combustion Science 23 (1997) 81–94.
[19] G.G. Szego, B.B. Dally, G.J. Nathan, Combustion and Flame 156 (2009) 429–438.

[20] R. Weber, J.P. Smart, W. vdKamp, Proceedings of the Combustion Institute 30 (2005) 2623–2629.
[21] J. Mi, P. Li, B.B. Dally, R.A. Craig, Energy and Fuels 23 (2009) 5349–5356.
[22] S. Kumar, P.J. Paul, H.S. Mukunda, Proceedings of the Combustion Institute 29 (2002) 1131–1137.
[23] S. Kumar, P.J. Paul, H.S. Mukunda, Combustion Science and Technology 179 (2007) 2219–2253.
[24] A.F. Colorado, B.A. Herrera, A.A. Amell, Bioresource Technology 101 (2010) 2443–2449.
[25] A. Effuggi, D. Gelosa, M. Derudi, R. Rota, Combustion Science and Technology 180 (2008) 481–493.
[26] M. Derudi, R. Rota, Proceedings of the Combustion Institute 33 (2011) 3325–3332.
[27] A.H. Lefebvre, Atomization and Sprays, Hemisphere, Washington DC, 1989.
[28] R. Hadef, B. Lenze, Chemical Engineering and Processing 47 (2008) 2209–2217.
[29] R. Hadef, B. Lenze, Experimental Thermal and Fluid Science 30 (2005) 117–130.
[30] A. Cavaliere, M. de Joannon, Progress in Energy and Combustion Science 30 (2004) 329–366.
[31] R.A. Yetter, I. Glassman, H.C. Gabler, Proceedings of the Combustion Institute 28 (2000) 1265–1272.
[32] A.E.E. Khalil, A.K. Gupta, Applied Energy 88 (2011) 3685–3693.
[33] V.M. Reddy, D. Sawant, D. Trivedi, S. Kumar, Proceedings of the Combustion Institute 34 (2013) 3319–3326.
[34] V.M. Reddy, S. Kumar, Propulsion and Power Research 2 (2013) 139–147.
[35] T. Daho, G. Vaitilingom, O. Sanogo, S.K. Ouiminga, B.G. Segda, J. Valette, P. Higelin, J. Koulidiati, Biomass and Bioenergy 46 (2012) 653–663.
[36] M.A. Hess, M.J. Haas, T.A. Foglia, Fuel Processing Technology 88 (2007) 693–699.
[37] J. Kamrak, B. Kongsombut, G. Grehan, S. Saengkaew, K. Kim, T. Charinpanitkul, Biomass and Bioenergy 33 (2009) 1452–1457.
[38] C.S. Yang, D.Z. Jeng, Y. Yang, H. Chen, C. Gau, Experimental Thermal and Fluid Science 35 (2011) 73–81.
[39] M. Choi, A. Hamins, G. Mulholand, T. Kashiwagi, Combustion and Flame 102 (1995) 161–169.
[40] H.F. Gercel, Biomass and Bioenergy 23 (2002) 307–314.
[41] C. Ilkılıç, S. Aydın, R. Behcet, H. Aydin, Fuel Processing Technology 92 (2011) 356–362.
[42] V.M. Reddy, Flameless combustion with liquid fuels, (Ph.D Thesis) Indian Institute of Technology Bombay, India, 2013.
[43] P. Manna, M. Dharavath, P.K. Sinha, D. Chakraborty, Aerospace Science and Technology 27 (2013) 138–146.
[44] A.S. Veríssimo, A.M.A. Rocha, M. Costa, Fuel Processing Technology 106 (2013) 423–428.
[45] A. Wulff, J. Hournouziadis, Aerospace Science and Technology 8 (1997) 557–572.
[46] R.A. Yetter, F.L. Dryer, H. Rabitz, Combustion Science and Technology 79 (1991) 97–128.
[47] Y.D. Wang, Y. Huang, D. McIlveen-Wright, J. McMullan, N. Hewitt, P. Eames, S. Rezvani, Fuel Processing Technology 87 (2006) 727–736.
[48] M. Moghiman, T.M. Greunberger, P.J. Bowen, N. Syred, Combustion Science and Technology 174 (2002) 67–86.